Transverse beam stability with an ''electron lens''

A. Burov,* V. Danilov,† and V. Shiltsev
Fermi National Accelerator Laboratory, Batavia, Illinois 60510
(Received 29 July 1998)

This article is devoted to stability analysis of the antiproton beam interacting with an electron beam in an ''electron lens'' setup for beam-beam compensation in the Tevatron collider. Electron space charge forces cause transverse ''head-tail'' coupling within antiproton bunch which may lead to a transverse mode coupling instability (TMCI). We present a theory, analytical studies, and numerical simulations of this effect. An estimate of threshold longitudinal magnetic field necessary to avoid the instability is given. Dependence of the threshold on electron and antiproton beam parameters is studied. [S1063-651X(99)10203-4]

PACS number(s): 41.75.Lx, 29.27.Bd

I. INTRODUCTION

Proton and antiproton beams in the Tevatron collider interact via their electromagnetic forces at two collision points B0 and D0, and at numerous locations along separated orbits in the same vacuum chamber where they near miss each other. Such an interaction causes betatron oscillation tune shift and tune spread in both beams. The tune shift and the tune spread are supposedly much larger in the antiproton beam than in the proton one, because the proton intensity is several times larger, and can reach values of about 0.01-0.02 in the Tevatron luminosity upgrade project TEV33 [1]. These effects are expected to be a problem for the machine operation if uncorrected. Compensation of the beam-beam effects in the Tevatron with use of a high current, low energy electron beam was proposed in Refs. [2–4]. The electron beam travels in the direction opposite to the antiproton beam and interacts with an antiproton bunch via its space charge forces. The proton beam has to be separated from the electron and antiproton beams. Implementation of the proposal are (1) the ''electron lens'' with modulated current to provide different linear defocusing forces for different antiproton bunches (the bunch spacing is $\tau = 132$ ns in the TEV33) in order to equalize their betatron frequencies which are not naturally equal due to proton-antiproton interaction in numerous parasitic crossings along the ring; and (2) the ''electron compressor,'' that is nonlinear dc electron lens to compensate (on average) the nonlinear focusing due to the proton beam.

The electron beam setup is to be installed away from the proton-antiproton interaction points at B0 and D0 and could look much like an ''electron cooler'' (see, e.g. [5]), except electrons collide with antiprotons. The negative tune shift of the antiprotons ($\bar{p}$s) due to a round, constant density electron beam with total current J_e, radius a_e, interacting with antiprotons over a length L_e, is equal to [3]

$$\xi^e_{x,y} \approx -\frac{\beta_{x,y}}{4\pi}\frac{2(1+\beta_e)J_e L_e r_{\bar{p}}}{e v_e a_e^2 \gamma_{\bar{p}}}, \tag{1}$$

here $r_{\bar{p}} = e^2/(M_{\bar{p}}c^2) \approx 1.53\times 10^{-18}$ m is the (anti)proton classical radius, $\gamma_{\bar{p}}$ is relativistic antiproton factor, $v_e = c\beta_e$ is electron beam velocity, $\beta_{x,y}$ is the beta function at the set-up location (x for horizontal, y for vertical). For example, $L_e = 2$ m long set-up with $J_e = 1.5$ A current of 10 kV electrons ($\beta_e = 0.2$) installed at $\beta_x = 100$ m can shift the horizontal tune of the 1 TeV antiprotons by $\xi^e_x \approx -9.1\times 10^{-3}$ if the electron beam radius is $a_e = 1$ mm. Strong longitudinal magnetic field plays a significant role in maintaining stability of both electron and antiproton beams [6]. It also suppresses the electron beam current distribution distortions and, therefore, the electron space charge force distortions [7].

Low energy electrons can create significant transverse impedance comparable with intrinsic impedance of the Tevatron ring, that can result in collective instabilities of the antiproton bunch. The electron beam is generated by an electron gun cathode, transported through the interaction region, and absorbed in the collector. Therefore, each portion of electrons passes through the $\bar{p}$ beam only once, and only short distance transverse wake fields are of interest. The most important collective effect is similar to the ''strong head-tail'' interaction, considered, e.g., in [8]. It is assumed that the Tevatron ring chromaticity can be made close to zero, so the increments of so-called ''weak head-tail'' [8] instability are negligible.

In this article we study ''strong head-tail'' instability in the $\bar{p}$ beam caused by wide band impedance due to the electron beam. The phenomenon takes place if, for example, the centroid of the bunch head collides off the electron beam center. Electron-antiproton repulsion causes electron motion and, as a result, the electron beam acquires a displacement at the moment when it interacts with the tail of the $\bar{p}$ bunch. Thus, the impact of the electron beam on the following antiprotons depends on the transverse coordinate of preceding $\bar{p}$s. The effect is similar to what is observed in electron storage rings where short range wake fields due to vacuum chamber discontinuities can lead to transverse mode coupling instability (TMCI) [8]. The TMCI in electron rings limits the maximum single bunch current. In our case, the

*On leave from Budker Institute of Nuclear Physics, Novosibirsk 630090, Russia.
†Present address: Oak Ridge National Laboratory, Oak Ridge, Tennessee 37831-8218.

source of the coupling is the electron space charge which is a basic mechanism for the beam-beam compensation and, thus, can not be avoided. The way to counteract the instability is to increase the electron beam rigidity, to make its motion during the collision smaller. Naturally it can be done using a strong longitudinal magnetic field in the interaction region.

Theoretical analysis of the ''head-tail'' stability in a two mode model is presented in Sec. II of this article. In Sec. III we analyze synchro-betatron modes of the antiproton bunch motion. Section IV is devoted to numerical simulations of the $\bar{p}$'s dynamics in the Tevatron with the ''electron lens.'' Finally, a brief summary is given in Sec. V.

II. TWO MODE MODEL

A. Direct and skew wakes

Conventionally, the analysis of relativistic beam stability relies on the wake function concept, see, e.g., [8]. Electromagnetic fields excited in accelerator vacuum pipes vary over transverse distances of about the pipe aperture b, which is usually much larger than the beam radius a. That allows the perturbation to expand on the dipole, quadrupole, and higher order terms over the small parameter (a/b).

The situation is different for the case under study. The electron beam space charge fields excited by antiprotons have about the same transverse extent as the $\bar{p}$ beam, that complicates the analysis. However, the interaction can be described by the conventional approach for a specific case when both $\bar{p}$ and electron bunches are homogeneous and bounded by the same radius $a=a_e=a_{\bar{p}}$. Now electromagnetic wake fields have a simple radial structure, they can be easily calculated and used in the conventional formalism of the wake functions.

To find the dipole wake function, let us consider a thin antiproton slice with a charge q and transverse offset Δx traveling through the electron beam. After interaction with the slice, electrons acquire a transverse velocity

$$v_{xe}=\frac{2eq\Delta x}{a^2\gamma_e mc}, \tag{2}$$

where m is the electron mass. Such a kick causes transverse Larmor oscillations in a longitudinal magnetic field B, and after a time interval t, the resulting electron transverse offsets are

$$x_e=\frac{v_{xe}}{\omega_L}\sin(\omega_L t); \quad y_e=\frac{v_{xe}}{\omega_L}(1-\cos(\omega_L t)), \tag{3}$$

where $\omega_L=eB/(\gamma_e mc)$ stands for the Larmor frequency, and $\gamma_e=1/\sqrt{1-\beta_e^2}$. Numerical simulation of these oscillations of the electron beam are presented below in Sec. IV; see Fig.4. One can see that the originally horizontal displacement Δx resulted in both horizontal and vertical displacements. Taking into account the possibility of a vertical offset y, we conclude that antiprotons at the distance s behind the slice will experience momentum changes equal to

$$\Delta p_x(s)=-\frac{eq}{c}(W_d(s)\Delta x-W_s(s)\Delta y),$$

$$\Delta p_y(s)=-\frac{eq}{c}(W_s(s)\Delta x+W_d(s)\Delta y), \tag{4}$$

where we introduced direct wake function $W_d(s)$ and skew $W_s(s)$ wake function:

$$W_d(s)=W\sin(ks), \quad W_s(s)=W(1-\cos(ks)), \tag{5}$$

$W_{d,s}(s)=0$, if $s\leqslant 0$, and

$$W=\frac{4\pi n_e L_e}{Ba^2}, \quad n_e=\frac{J_e}{\pi a^2 v_e}, \quad k=\frac{\omega_L}{(1+\beta_e)c}. \tag{6}$$

Depending on the parameters, one or the other of the two wake functions (5) can give a dominant influence on the antiproton beam stability. As we will show below, the direct wake effects are suppressed if there are many Larmor oscillations periods over the $\bar{p}$ bunch length σ_s, while the skew force impact decreases with increasing the x-y detuning.

To be precise, the influence of the space charge due to the unperturbed antiproton distribution has to be taken into consideration when we calculate the wake functions. Radial electric and azimuthal magnetic fields of the antiproton bunch $E_{\bar{p}},H_{\bar{p}}$ cause slow azimuthal drift of electron Larmor circles (3) around the antiproton beam axis. The typical drift angle over the antiproton rms bunch length is $\theta_d=[(E_{\bar{p}}+\beta_e H_{\bar{p}})/Br]\sigma_s=N_{\bar{p}}/\sqrt{2\pi}(B/e)a^2$. As a consequence the direct wake function acquires nonoscillating term. Under parameters of interest, $N_{\bar{p}}=6\times 10^{10}$, $a=1$ mm, $B=20$ kG, the angle is small $\theta_d=0.05$. The drift effect will be neglected in the two-mode analysis because θ_d is much smaller than the skew-coupling parameter $\simeq\sqrt{\nu_s/(\nu_x-\nu_y)}\simeq 0.3$ (see below). Nevertheless, numerical simulations in Sec. IV are free of such a simplification and take the effect into account.

B. Mode coupling

Let us write down single particle equations of motion along the accelerator orbit:

$$\frac{d^2x}{d\theta^2}+k_x(\theta)x=F_x(\theta), \quad \frac{d^2y}{d\theta^2}+k_y(\theta)y=F_y(\theta) \tag{7}$$

here $\theta=s/R=\omega_0 t$ is azimuth coordinate, R is the average ring radius, and $\omega_0=c/R$ is the revolution frequency. The accelerator focusing lattice is represented by terms $k_{x,y}$. The forces $F_{x,y}(\theta)$ are due to additional fields on the antiproton orbit. Equation (7) can be presented in terms of slow amplitudes X,Y determined as

$$x=X\ \exp\left(-i\int^{\theta}\frac{d\theta' R}{\beta_x(\theta')}\right)+\text{c.c.},$$

$$dx/d\theta=-iX\frac{R}{\beta_x(\theta)}\exp\left(-i\int^{\theta}\frac{d\theta' R}{\beta_x(\theta')}\right)+\text{c.c.}, \tag{8}$$

and similarly in y direction. Here $\beta_{x,y}(\theta)$ are horizontal and vertical beta-functions. Assuming the forces $F_{x,y}$ being lo-

calized within a small azimuthal interval where beta functions are $\beta_{x,y}$, we get from Eq. (8) the equations for the amplitudes X,Y:

$$\frac{dX}{d\theta}=\frac{i\beta_x}{2R}F_x\ \exp(i\nu_x\theta),\ \ \frac{dY}{d\theta}=\frac{i\beta_y}{2R}F_y\ \exp(i\nu_y\theta), \quad (9)$$

where $\nu_{x,y}=\int_{-\pi}^{\pi}[d\theta' R/\beta_{x,y}(\theta')]$ are the betatron tunes.

For the typical parameters of the electron compressor, the Larmor phase advance ϕ_L over the rms pbar bunch length σ_s is very large. For example, taking $B=10$ kG, $\beta_e=0.2$, $\sigma_s=30$ cm, one gets $\phi_L=k\sigma\approx 23\times 2\pi$. As we will estimate later, the fast oscillating terms in the wake forces (5) give insignificant effect in the slow amplitudes, and we can limit our consideration with only steplike term $W_s(s)=W$. Using the ''hollow-beam'' model [8] which assumes the same synchrotron oscillation amplitude for all particles, we get the following expressions for the forces:

$$F_x(\theta)=-\delta_P(\theta)\mathcal{F}\int_{-|\psi|}^{|\psi|}y(\psi')d\psi',$$

$$F_y(\theta)=\delta_P(\theta)\mathcal{F}\int_{-|\psi|}^{|\psi|}x(\psi')d\psi', \quad (10)$$

$$-\pi\leqslant\psi\leqslant\pi,\quad \mathcal{F}=\frac{Wr_p^-N_p^-R}{2\pi\gamma_p^-},$$

where ψ is the synchrotron phase and $\delta_P(\theta)$ is the periodic δ function with $\int_{-\pi}^{\pi}\delta_P(\theta)d\theta=1$. Equations (9) can be solved with the substitution

$$d/d\theta=\partial/\partial\theta+\nu_s\partial/\partial\psi, \quad (11)$$

where ν_s is the synchrotron tune.

The result of the integration depends on the vicinity of the synchrobetatron resonances $\nu_x\pm\nu_y+k\nu_s=l$, where k, l are integer numbers. If the number k of the nearest sum resonance is high enough, then the influence of the resonance can be neglected. It is equivalent to a drop of the complex conjugated terms in Eq. (8). The solutions are expanded now over the unperturbed synchrotron modes:

$$X=\exp(i\tilde{\nu}_x\theta)\sum_{m=-\infty}^{\infty}x_m\ \exp(im\psi),$$

$$Y\exp(-i\tilde{\nu}_x\theta)\sum_{n=-\infty}^{\infty}y_n\ \exp(in\psi), \quad (12)$$

where $\tilde{\nu}_{x,y}$ stand for fractional parts of the tunes. Below, these modes are referred to as $|xm\rangle,|yn\rangle$. Eigenvectors $x_m,y_n\propto\exp(-i\nu\theta)$ and eigenvalues ν to be found from the following set of algebraic equations:

$$x_m=-\frac{\mathcal{F}\beta_x}{2R(\tilde{\nu}_x-\nu+m\nu_s)}\sum_n C_{mn}y_n,$$

$$y_n=\frac{\mathcal{F}\beta_y}{2R(\tilde{\nu}_y-\nu+n\nu_s)}\sum_l C_{nl}x_l, \quad (13)$$

$$C_{mn}=\int_{-\pi}^{\pi}\frac{d\psi}{2\pi}\int_{-|\psi|}^{|\psi|}\frac{d\psi'}{2\pi}\exp(-im\psi+in\psi').$$

The matrix elements are presented below:

$$C_{mn}=\frac{1}{2\pi^2 n}\left(\frac{1-(-1)^{n+m}}{n+m}+\frac{1-(-1)^{n-m}}{n-m}\right)$$

$$\text{for}\ \ n\neq 0,\pm m,$$

$$C_{m0}=-\frac{1-(-1)^m}{\pi^2m^2}\quad \text{for}\ \ m\neq 0, \quad (14)$$

$$C_{mn}=0,\quad \text{for}\ \ n=\pm m\neq 0,$$

$$C_{00}=1/2.$$

Generally, Eqs. (13) may have unstable solutions when the coherent interaction $\propto\mathcal{F}$ is strong enough to couple the unperturbed synchrotron modes. There are possibilities to couple a pair of modes which belong to the same plane (vertical or horizontal) or to different planes. For example, if $\nu_y<\nu_x$, then, with an increase of the interaction parameter $\mathcal{F}$, the first pair of the same polarity modes to couple is $|y0\rangle$ and $|y1\rangle$. The motion in x plane may be considered as a forced motion at the frequency $\tilde{\nu}_y$, which makes the x equation (13) independent on the sought-for frequency ν. Substitution of the x equation (14) into the y equation yields

$$(\tilde{\nu}_y-\nu+n\nu_s)y_n+\alpha\nu_s\sum_m G_{nm}y_m=0,$$

$$\alpha=\mathcal{F}^2\beta_x\beta_y/(4R^2\Delta\nu\nu_s),\quad G_{nm}=\sum_l C_{nl}C_{lm}, \quad (15)$$

where $\Delta\nu=\nu_x-\nu_y$. Neglecting the contribution of all the modes apart from the coupled ones $|y0\rangle,|y1\rangle$ results in a quadratic equation on the eigenfrequencies. The solutions of the equation are real when the following threshold condition is satisfied:

$$\alpha\leqslant\alpha_S=(1/4+2/\pi^2-4/\pi^4)^{-1}\approx 2.43 \quad (16)$$

that leads to

$$\mathcal{F}\leqslant\mathcal{F}_S=2R\sqrt{\alpha_S\Delta\nu\nu_s/(\beta_x\beta_y)}\approx 3.12R\sqrt{\Delta\nu\nu_s/(\beta_x\beta_y)}. \quad (17)$$

This condition can be also expressed in terms of threshold magnetic field:

$$B\geqslant B_{th}\approx 1.3\frac{eN_p^-\sqrt{\xi_x\xi_y}}{a^2\sqrt{\Delta\nu\nu_s}}. \quad (18)$$

For $\xi_x=\xi_y=0.01$, $N_p^-=6\times 10^{10}$, $\nu_s=0.001$, $\Delta\nu=0.01$, $a=1$ mm it comes out $B_{th}=12$ kG.

Other solutions of Eqs. (13) are associated with the coupling of x and y modes. The most dangerous case is realized in the vicinity of the resonance $\nu_x+m\nu_s=\nu_y+n\nu_s$; then the quadratic equation for the eigenfrequency is as follows:

$$(\nu-\tilde{\nu}_x-m\nu_s)(\nu-\tilde{\nu}_y-n\nu_s)=\frac{-\mathcal{F}^2\beta_x\beta_y}{4R^2}C_{mn}C_{nm}. \tag{19}$$

The stability condition reads

$$(\tilde{\nu}_x-\tilde{\nu}_y-m\nu_s-n\nu_s)^2\geqslant(\mathcal{F}^2\beta_x\beta_y/R^2)C_{mn}C_{nm}. \tag{20}$$

Apart from C_{00}, all nonzero matrix elements C_{mn} (14) change sign after the transposing, thus, the right hand side of Eq. (20) is negative and the condition is satisfied. Therefore, only $|x0\rangle-|y0\rangle$ coupling can result in an instability. To avoid it, the interaction constant $\mathcal{F}$ has to be small enough:

$$\mathcal{F}\leqslant 2R|\Delta\nu|/\sqrt{\beta_x\beta_y}. \tag{21}$$

This stability condition can more stringent than the previous one (17) if $|\Delta\nu|\leqslant\alpha_S\nu_s$. The corresponding instability does not involve head-tail modes, does not depend on the synchrotron tune, and is a single particle dynamics effect.

The fast oscillating direct wake function $W_d(s)$ (5) gives the matrix elements suppressed as $\propto 1/(k\sigma_s)$. As a result, the threshold value of the interaction parameter $\mathcal{F}$ for the direct instability $\mathcal{F}_D$ occurs to be much higher then the skew one $\mathcal{F}_S$:

$$\mathcal{F}_D/\mathcal{F}_S\simeq k\sigma_s\sqrt{\nu_s/\Delta\nu}\gg 1. \tag{22}$$

Therefore, it is the constant skew wake that plays a major role in the mode coupling.

C. Scaling with electron beam radius

Let us consider an electron beam with radius larger than the antiproton beam radius, $a_e\gg a_{\bar{p}}$. To find out how the direct and skew wake functions scale with the electron beam radius, we start with the continuity equation for the electron media:

$$\frac{\partial\rho_e}{\partial t}+\vec{\nabla}\cdot(n_e\vec{v}_e)=0, \tag{23}$$

where n_e and ρ_e are the electron density and its perturbation, $\vec{v}_e$ is the electron velocity. Dealing with the antiproton slice of charge q and offset Δx which causes ρ_i and corresponding the electric field $\vec{E}_i$, we get

$$\rho_i(x,y,s)=\frac{\Delta x x q}{r}\frac{dn_i}{dr}\delta(s),$$

$$\vec{\nabla}\cdot\int ds\vec{E}_i(s)=-4\pi e\int ds\rho_i(s), \tag{24}$$

$$\int d\vec{r}n_i(r)=1,\quad r^2=x^2+y^2$$

and all the vectors, including $\vec{\nabla}$, are transverse two-dimensional ones.

Just after the kick, the electron velocity $\vec{v}_e(0)$ is

$$\vec{v}_e(0)=cr_e\int ds\vec{E}_i(s)/e. \tag{25}$$

Then, the awaken electron velocity undergoes the Larmor rotation:

$$\vec{v}_e(t)=\hat{T}(t)\vec{v}_e(0), \tag{26}$$

with the rotation transformation matrix of

$$\hat{T}(t)=\begin{pmatrix}\cos(\omega_L t) & -\sin(\omega_L t)\\ \sin(\omega_L t) & \cos(\omega_L t)\end{pmatrix}. \tag{27}$$

Collecting these equations altogether and denoting $\vec{r}_e(t)=\int_0^t dt\vec{v}_e(t)$, it comes out

$$\rho_e=-n_e\vec{\nabla}\cdot\vec{v}_e(0)\sin(\omega_L t)/\omega_L-\vec{r}_e(t)\cdot\vec{\nabla}n_e. \tag{28}$$

The first term in the right hand side of the last equation leads to the oscillating direct wake function. It is determined by the electron density at the location of the antiproton beam and is not influenced by the remote boundary of the electron beam. So it may be concluded that the oscillating direct wake does not depend on the electron beam radius when the electron density is fixed. Equation (5) gives an estimate for this wake function.

The second term in Eq. (28) contains the non-oscillating drift part $\vec{r}_e=\vec{v}_e(0)\times\vec{\omega}_L/\omega_L^2$ and, actually, describes the constant part of the skew wake. Mostly, the electron boundary contributes to this term as it is $\propto\vec{\nabla}n_e$. To see its scaling with the electron beam radius a_e, one notes that the field of the dipole perturbation drops quadratically with the radius $E_i(\vec{r})\propto 1/r^2$. Consequently, the constant wake function goes down the same way

$$W_s\propto n_e/a_e^2. \tag{29}$$

Thus, an increase of the electron beam radius can be used to suppress the skew instability.

III. MULTIMODE ANALYSIS

The two mode model presented in the previous section allowed to derive analytical formulas for the TMCI threshold taking into account only the constant skew component of the wake force due to the electron beam and just two coupling modes. More general numerical algorithm for calculating the mode coupling developed in Ref. [9] allows to avoid such simplifications and consider many modes and general wake form, and, important, deals with nonaveraged motion. For that the antiproton bunch is divided into several radial and azimuthal parts in the synchrotron phase space, and consequently, a series of synchrobetatron modes can be seen. The wake force kick changes the backward particles angles, while the rest of the accelerator is represented by a linear transformation matrix (rotation in phase space). Eigenvalues (eigentunes) of the resulting transformation matrix can be calculated numerically. Complexity of the calculations is squared the number of modes, so, for calculations with MATHCad software one has to limit the number.

We divide the bunch in 1 radial (i.e., the same synchrotron oscillations amplitude for all particles) and 7 azimuthal parts for both vertical and horizontal degrees of freedom, so it is possible to see the behavior of the first 1 radial and 7

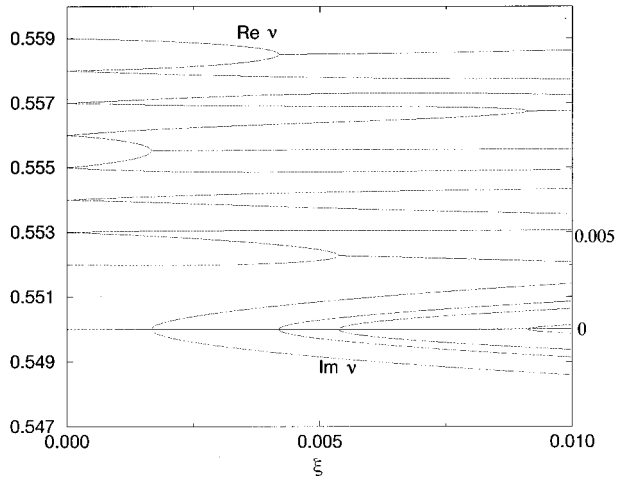

FIG. 1. Eigenfrequencies (tunes) of the antiproton bunch oscillation modes versus the antiproton betatron tune shift due to electron beam ξ_e (horizontal axis). Vertical scale on the left is for fractional part of the tunes Re ν (upper series of lines), the right side scale is for imaginary part of the tunes Im ν (lower series of lines).

azimuthal synchrobetatron modes in horizontal and vertical motion with taking into account their coupling. Complete expressions for the linearized direct and skew transverse wake functions Eq. (5) are used.

Numerical parameters used in these calculations are $N_{\bar{p}}=6\times10^{10}$, the rms size of round Gaussian antiproton beam is $\sigma_{\bar{p}}=1$ mm, the longitudinal magnetic field is equal to 10 kG. Figure 1 shows the eigentunes versus the linear betatron tune shift ξ_e due to interaction with electron beam while the fractional part of the betatron tune for the horizontal motion is equal to $\nu_x=0.556$ and for the vertical one $\nu_y=0.555$, the synchrotron tune is 0.001, therefore, the betatron tunes difference is exactly the synchrotron tune. If $\xi_e=0.0$, then the eigenfrequencies of the azimuthal modes are equal to $\nu_{x,y}+k\nu_s$, where integer k has 7 values in the range of $-3,\ldots3$ and represents the number of modulation periods in the synchrotron phase space. Some of the modes are coupling with increase of ξ_e, real parts of their tunes Re ν (see upper series of curves in Fig. 1) become equal, while imaginary parts Im ν become one negative and another positive. The latter evidently means instability in the motion. In our case, the first merging of modes takes place at $\xi\approx0.0017$; the next merging of higher modes occurs at $\xi\approx0.0045$, etc.

Next Fig. 2 shows the tune shift threshold ξ_e for the first coupling modes versus the tune split in units of the synchrotron tune $\Delta\nu=(\nu_x-\nu_y)$ while the vertical tune is equal to 0.555. The threshold grows linearly until $\Delta\nu\approx(2-2.5)\nu_s$ and then is approximately proportional to $\sqrt{\Delta\nu}$, in a good agreement with the two mode model formulas (18) and (21). Note, that completely adequate consideration of the fast oscillating parts of the wakes would require many more modes $\sim k\sigma_s\simeq30-100$ to be taken into account.

IV. SIMULATIONS

A. The code

Three dimensional numerical simulations of the effects have been done with ECWAKE code written in FORTRAN.

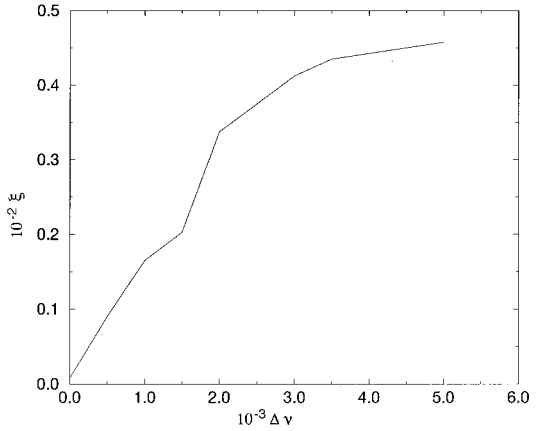

FIG. 2. Threshold antiprotons tune shift ξ_e (vertical axis) due to the electron beam versus the difference of antiproton horizontal and vertical tunes $\Delta\nu=\nu_x-\nu_y$. $B=10$ kG, $\nu_s=0.001$, and $N_{\bar{p}}=6\times10^{10}$.

The $\bar{p}$ beam is represented as a number of macroparticles (typically in the range from $M=128$ to maximum 2048). The particles have equal charges $e\Delta N_{\bar{p}}=eN_{\bar{p}}/M$. Numerical procedure to generate the longitudinal phase space distribution starts with pairs of numbers $(t_i,u_i),i=1,\ldots,M$ uniformly distributed in a unit circle, then the longitudinal position of ith particle τ_i and its derivative $\upsilon_i=d\tau_i/(dt\cdot\nu_s\omega_0)$ are derived as

$$(\tau_i,\upsilon_i)=L(t_i,u_i)\sqrt{\frac{1-(1-t_i^2-u_i^2)^{1/(1+\mu)}}{t_i^2+u_i^2}},\qquad(30)$$

where $2L$ is the maximum bunch length, and the parameter μ determines the bunch shape. The smoothed density in longitudinal phase space is proportional to $(L^2-\tau^2-\upsilon^2)^\mu$, and the corresponding line density is proportional to $(L^2-\tau^2)^{\mu+1/2}$. Figure 3 shows an example of the longitudinal distribution of 1024 particles generated with use of Eq.(30) with $\mu=1.5$.

Initial distribution of particles transverse coordinates and velocities does not play a big role in the development of the subject instability, and usually we either assign the same displacement to all particles or use 2D Gaussian numbers for

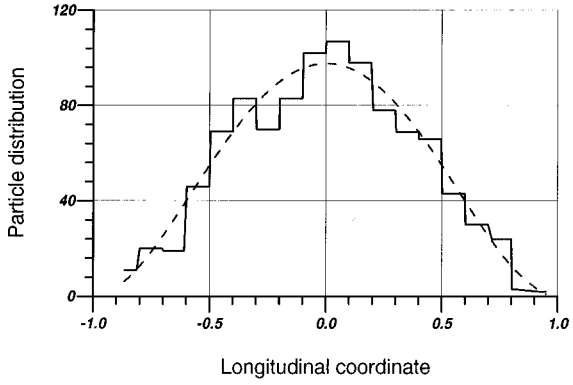

FIG. 3. Longitudinal distribution of 1024 macroparticles in antiproton bunch generated according to Eq. (30) with $\mu=1.5$. Dashed line is for $(L^2-\tau^2)^{\mu+1/2}$.

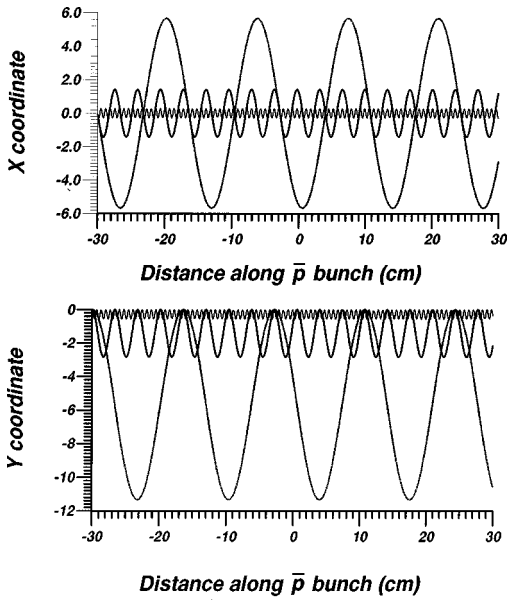

FIG. 4. Electron beam motion due to displaced $\bar{p}$ slice in solenoid magnetic field of $B=1$, 4, and 20 kG.

x_i, y_i, v_{xi}, v_{yi} (in the latter case, unstable motion starts from noise). During the simulation, the longitudinal variables are updated once per turn using a rotation with angle $2\pi\nu_s$, while the horizontal and vertical variables are rotated by $2\pi\nu_{xi}$ and $2\pi\nu_{yi}$, respectively. Generally, the transverse tunes are not the same for all particles—instead, one can distribute them uniformly with maximum deviation of $\pm\delta\nu$ around mean values of $\nu_{x,y}$.

At every turn the particles collide with an electron beam, and, therefore, excite Larmor motion of the electron beam. In simulation, the electrons' angular kick due to antiprotons is used in linear approximation:

$$\vec{\Delta}\theta_e = \frac{\vec{\Delta}p_{e\perp}}{\gamma_e mc\beta_e} \approx -\frac{\Delta N_{\bar{p}} r_e}{\gamma_e \beta_e \sigma_{\bar{p}}^2}(\vec{r_{\bar{p}}} - \vec{r_e}), \tag{31}$$

where $\sigma_{\bar{p}}$ is the rms size of round Gaussian antiproton beam, $r_e = 2.82\times10^{-15}$ m is electron classical radius, and vectors $\vec{r_{\bar{p}}}, \vec{r_e}$ denote positions of antiproton slice and electron beam centroid, respectively. Every such a kick results in Larmor oscillations of electrons. Note, that due to Gaussian distribution function, the kick (31) has no numerical factor 2 as in Eq. (2) and $\sigma_{\bar{p}}$ is used instead of a.

Figure 4 demonstrates the electron beam displacement x_e, y_e behind the only macroparticle at the $\bar{p}$ bunch head (at $s=-30$ cm) displaced in x plane in longitudinal field of $B=1$,4 and 20 kG. One can see, that amplitude and period of the Larmor oscillations are both inversely proportional to B: larger amplitude oscillations are for $B=1$ kG, the smallest amplitude is seen for 20 kG, and the 4 kG solenoid field case is intermediate. The motion in y plane has nonzero mean component if the original displacement is in x plane (and vice versa)—that is the skew impedance source discussed in Sec. II.

All preceding macroparticles contribute to the electron beam displacement which is seen by a subsequent macroparticle. (In particular, this is the reason of the slow drift contribution discussed in Sec. II.) As a result, the angular kick due to the electron beam depends on the macroparticle position τ:

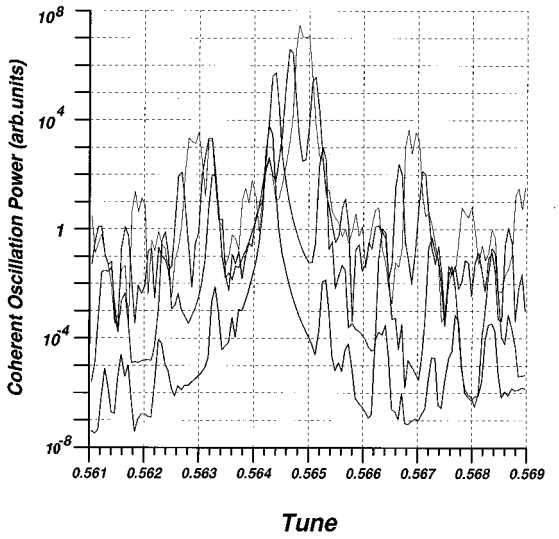

FIG. 5. Antiproton oscillations spectra with different solenoid field $B=18$, 20, 40, and 400 kG. $\nu_x=0.585$, $\nu_y=0.575$, $\nu_s=0.001$, $\xi_e=-0.01$, $\delta\nu=0$, $N_{\bar{p}}=6\times10^{10}$, and $\bar{p}$ beam $\sigma_{\bar{p}}=0.7$ mm.

$$\Delta x'_{\bar{p}}(\tau) = -\frac{4\pi\xi_e}{\beta_x}(x_e(\tau) - x_{\bar{p}}(\tau)), \tag{32}$$

with a similar formula for the y plane; ξ_e is given in Eq. (1). At every turn we use a standard fast algorithm [10] for sorting the values τ_i so that $\tau_i \leqslant \tau_{i+1}$. It is based on ''doubling strategy'' and requires $M\ \log_2 M$ operations. Calculation of the kicks Eq. (32) needs accumulation of Larmor perturbations of the electron beam to obtain $x_e(\tau_i)$ that is done with another fast algorithm (of the order of $M\ \log_2 M$ operations) similar to phasor technique described, e.g., in [8,11]. The code allowed to track all variables involved, e.g. coordinates of any macroparticle and $\bar{p}$ beam centroid coordinates, motion of the electron beam parts, etc.

We have tested the code with a specific analytical model of the TMCI with constant wake function where the kick is equal to

$$\Delta x'_i = \frac{W_0}{M}\sum_{j\leqslant i} x_j .$$

If all macroparticles have the same synchrotron amplitude (often called ''hollow'' beam model), then theory [12] predicts threshold value of $W_0^{thr} \approx 14\nu_s$ for small synchrotron tunes $\nu_s \ll 1$ which does not depend on the bunch length – and that is what we have revealed with our code.

B. Simulation results

Figure 5 presents spectra of horizontal motion of the antiproton bunch centroid over 16 384 turns. Several curves correspond to solenoid field B while antiproton parameters are the same: number of macroparticles $M=1024$, constant

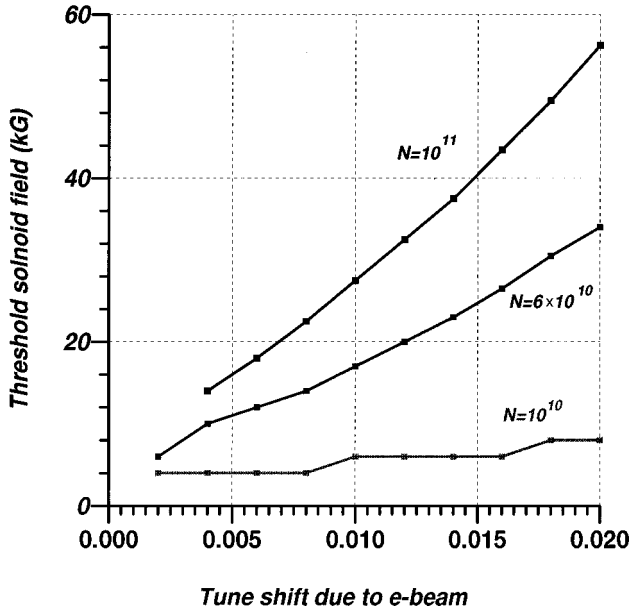

FIG. 6. Threshold solenoid field B_{thr} vs tune shift due to electrons $|\xi_e|$ at different bunch populations $N_{\bar{p}}=1$, 6, 10×10^{10}. Focusing lattice tunes $\nu_x=0.585$, $\nu_y=0.575$, synchrotron tune $\nu_s=0.0012$, maximum tune spread $\delta\nu=0$, and the rms size of $\bar{p}$ beam $\sigma_{\bar{p}}=0.7$ mm.

longitudinal charge distribution (30) with $\mu=-1/2$ and $L=70$ cm, $N_{\bar{p}}=6\times10^{10}$, $\sigma_{\bar{p}}=0.7$ mm, unperturbed lattice tunes are close to the Tevatron ones $(\nu_{x0},\nu_{y0})=(0.585,0.575)$, nominal tune shift due to electron beam $\xi^e_{x,y}=\xi_e=-0.01$, synchrotron tune $\nu_s=0.001$, and no betatron tune spread $\delta\nu=0$.

The wake field strength W from Eq. (6) is inversely proportional to B, thus, the spectrum corresponding to the highest $B=40$ T—see the lowest curve in Fig. 5—the only strong line at $\nu_x\approx\nu_{x0}+\xi_e\approx0.5644$ and several weak lines are shifted on integer number of synchrotron tunes, in particular, the first upper synchrotron side-band at $\nu_x+\nu_s$. Weaker magnetic field leads to stronger wake because larger Larmor motion of electrons is exited. As a result, synchrotron side-bands become stronger—see next two curves one above another in the figure, corresponding to $B=4$T and 2T, respectively. Simultaneously, frequencies of some modes, e.g., ν_x and $\nu_x+\nu_s$ shift toward each other. At the threshold value of $B_{thr}\approx1.8$ T, these lines merge, see the upper spectra in Fig. 5, the amplitude of the motion becomes very high, and any further decrease of B will lead to instability which develops over less than 16 384 turns to unacceptably high amplitudes for numerical tracking.

It is revealed, that although the $\bar{p}$ bunch motion is essentially two-dimensional (since the wake is 2D), the instability starts in that plane where the original lattice tune is closer to half integer $\nu=1/2$, e.g., in horizontal plane for the example discussed above.

Next Fig. 6 shows the threshold strength of solenoidal magnetic field B_{thr} vs electron beam intensity parameter ξ_e for antiproton bunch population equal to $N_{\bar{p}}=(1,6,10)\times10^{10}$—lower, middle and upper curves, respectively. We define the threshold as the value of B which results in more than 10-fold increase of the initial centroid betatron amplitude over the first 10 000 turns. One can see, that the field is approximately proportional to both ξ_e and $N_{\bar{p}}$ in accordance with theoretical prediction Eq. (18).

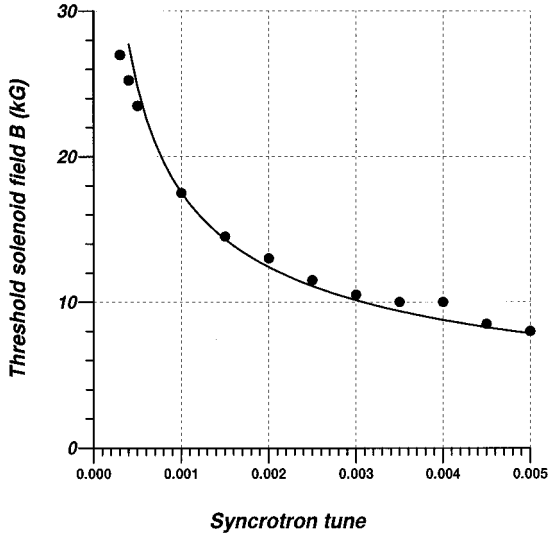

FIG. 7. Threshold magnetic field vs synchrotron tune ν_s. Solid line is for $B_{thr}=12.4[\mathrm{kG}]/\sqrt{\nu_s}$. $\nu_x=0.585$, $\nu_y=0.575$, $\xi_e=-0.01$, $\delta\nu=0$, $N_{\bar{p}}=6\times10^{10}$, and $\sigma_{\bar{p}}=0.7$ mm.

Dependence of the threshold on the synchrotron tune ν_s is depicted in Fig. 7. Dots are simulation results with $\nu_x=0.585$, $\nu_y=0.575$, $\xi_e=-0.01$, $\delta\nu=0.002$, $N_{\bar{p}}=6\times10^{10}$, $\sigma_{\bar{p}}=0.7$ mm. The solid line represents a fit $B_{thr}=17.5[kG]/\sqrt{\nu_s/0.001}$ in line with the two-mode prediction Eq. (18).

Contour plot of B_{thr} over range of synchrotron tunes $\nu_s=0.0002-0.002$ and $|\xi_e|=0.002-0.02$ is shown in Fig. 8 ($\nu_x=0.585$, $\nu_y=0.575$, other parameters are the same as above). One can see that B_{thr} varies from 12 kG to 48 kG over the parameter space. In order to evaluate the importance

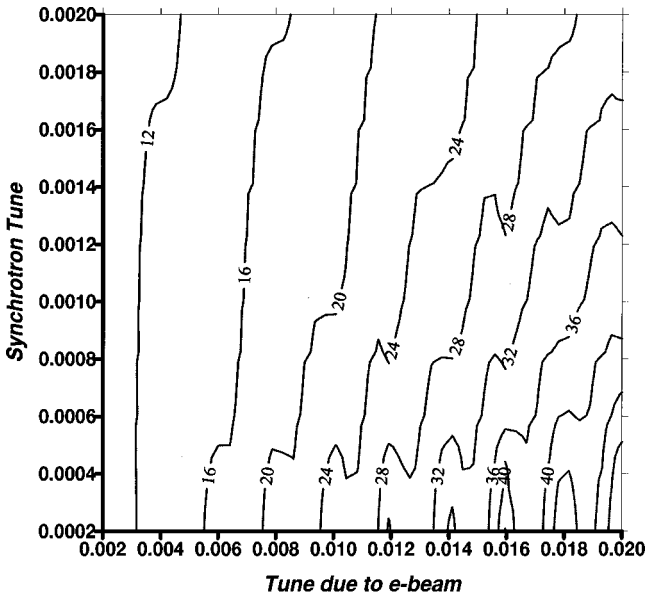

FIG. 8. Contour plot of the TMCI threshold magnetic field vs synchrotron tune ν_s and tune shift due to electrons $|\xi_e|$.

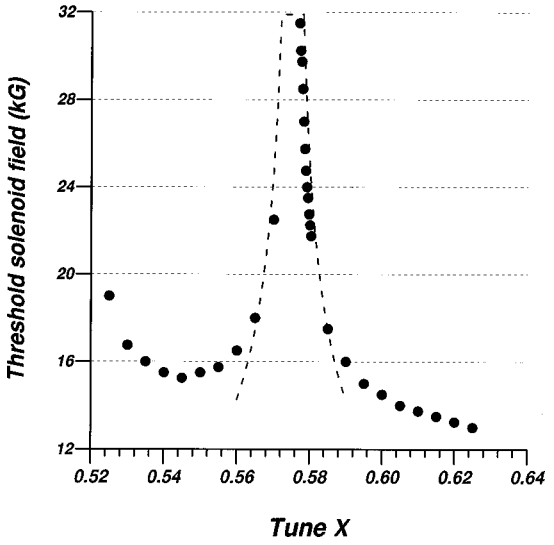

FIG. 9. Threshold magnetic field vs horizontal tune ν_x. Dashed line corresponds to $B_{thr} \propto 1/\sqrt{|\nu_x - \nu_y|}$; $\nu_y = 0.575$, $\nu_s = 0.001$, $\xi_e = -0.01$, $\delta\nu = 0.0$, $N_{\bar{p}} = 6 \times 10^{10}$, and $\sigma_{\bar{p}} = 0.7$ mm.

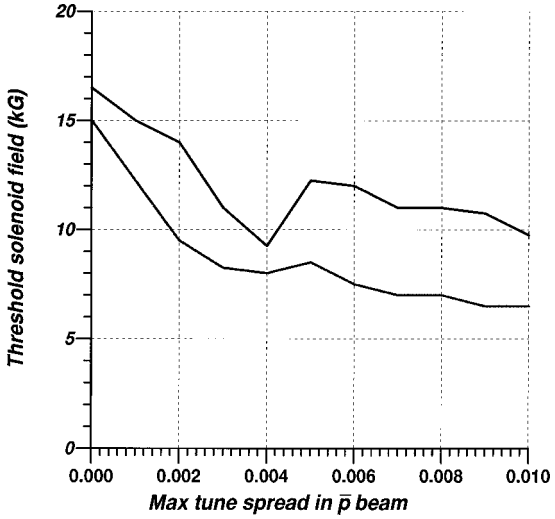

FIG. 10. TMCI threshold magnetic field vs maximum betatron tune spread $\delta\nu$ in the antiproton beam. $\Delta\nu = |\nu_x - \nu_y| = 0.585 - 0.575 = 0.01$ for the upper curve; and $\Delta\nu = 0.595 - 0.575 = 0.02$ for the lower curve. Synchrotron tune $\nu_s = 0.0012$, tune shift due to electrons $\xi_e = -0.01$, $N_{\bar{p}} = 6 \times 10^{10}$, and rms size of $\bar{p}$ beam $\sigma_{\bar{p}} = 0.7$ mm.

of the oscillation part of the wakes Eq. (5), we performed similar scan without the constant part of the skew wake, i.e., with $W_d(s) = W\sin(ks)$ and $W_s(s) = -W\cos(ks)$ and found that about 5 times smaller solenoid field is required for stability. It confirms the decisive role of the constant part of skew wake that is a basic assumption of the two-mode model in Sec. II.

It is found that the TMCI threshold greatly depends on operation point ν_x, ν_y. Figure 9 presents results of scanning of the horizontal tune ν_x from 0.52 to 0.63 while the vertical tune is $\nu_y = 0.575$. In close vicinity of the coupling resonance $\Delta\nu = |\nu_x - \nu_y| \leqslant 15\nu_s$ the threshold magnetic field depends on ν_s approximately as $\propto 1/|\Delta\nu|^{\kappa}$, where $2/5 < \kappa < 1/2$. Away from the resonance, the best fit power is $\kappa \approx 1/5$. The tune dependence on the tune split is different from Eq. (33) if $|\Delta\nu|$ is more than $15\nu_s \approx 0.015$. The threshold also goes up near half-integer resonance $\nu_x \to 0.5$.

In order to compare with the two mode model, one can fit B_{thr} in the form similar to Eq. (18):

$$B_{thr} \approx \frac{0.95 e N_{\bar{p}} \xi_e}{\sigma_{\bar{p}}^2 \sqrt{|\nu_x - \nu_y| \nu_s}} = \frac{(17.5\ \text{kG}) N_{\bar{p}}/6 \times 10^{10} |\xi_e/0.01|}{((\sigma_{\bar{p}}\ [\text{mm}])/0.7)^2 \sqrt{\nu_s/0.001 |\Delta\nu|/0.01}}; \quad (33)$$

see also dashed line in Fig. 9.

There is a difference in numerical factors between Eq. (33) and Eq. (18) which is probably because of (a) the kick (31) due to Gaussian beam has no numerical factor 2 as in Eq. (2), and $\sigma_{\bar{p}}$ is used instead of a; (b) oscillating parts of the wake forces and the effects of the drift of electrons in the space charge fields of the antiproton beam are taken into account in simulations in contrast to the two modes model; (c) more than two modes play a role in the computer tracking because of large number of macroparticles. At the same time, there is an excellent quantitative agreement with results of multimode analysis presented in Fig. 2.

Neither two-mode theory nor multimode analysis in Secs. II and III, respectively, deal with tune spread in the $\bar{p}$ bunch, though a general guess is that it has to ease the instability. In numerical simulations presented in Fig. 10, we tracked $M = 256$ macroparticles each having slightly different vertical and horizontal tunes spread in interval $\pm\delta\nu$ around their mean values $\nu_{x,y} = (0.585, 0.575)$, see the upper curve in the figure, and $\nu_{x,y} = (0.595, 0.575)$, see the lower curve. In both cases the tune spread helps to stabilize the TMCI and, e.g., if $\delta\nu \simeq |\Delta\nu|$ then the required B_{thr} is 1.5–2 times less than in the case of $\delta\nu = 0$. We need to note, that while macroparticles differ from each other by their longitudinal positions, the way we introduce the tune variation is equivalent to the tune spread *along* the bunch. In the Tevatron it can be caused by direct space charge in a bunched beam of $\bar{p}$s. The corresponding tune spread is about 0.001 at injection energy of 150 GeV, and, thus, comparable with synchrotron tune $\nu_s \approx 0.001 - 0.002$, but is negligible at the collision energy of 0.9–1 TeV as it scales as $\propto 1/\gamma_{\bar{p}}$.

Theoretical analysis made in Ref. [13] predicts a significant suppression of the TMCI due to Landau damping, caused by the tune spread *across* the beam if the latter is comparable or larger than synchrotron tune. That condition can take place in the Tevatron collider where the spread is due to beam-beam interaction and the nonlinearity of focusing lattice. Correct macroparticle tracking would require many particles in each macro slice, and, thus, a different code and presumably much more CPU time. This is a subject of further work. With our existing code we can mimic an effect of decoherence caused by the transverse tune spread, simply by introduction a decrement of betatron oscillations δ. The resulting instability threshold can be described by a fit Eq. (33) if one replaces $\nu_s \leftrightarrow \sqrt{\nu_s^2 + \delta^2}$.

V. CONCLUSIONS

We have considered ''strong head-tail'' instability of the Tevatron antiproton bunch due to the beam-beam compensa-

tion set-up. The ''head-tail'' interaction takes place when the electron beam is not rigid enough and can be displaced transversely by the bunch head particles. The resulting direct and skew wake forces act on the ''tail'' particles and, thus, can lead to the instability. We pursue three approaches to study the instability: a simple twomode coupling theoretical model, more sophisticated multimode analysis which requires numerical solution of eigenmode equations, and straightforward macroparticle computer simulation. The results coincide qualitatively and rather well quantitatively agree with each other. For the parameters of the planned Tevatron beam-beam compensation experiment the $\bar{p}$ bunch intensity $eN_{\bar{p}}=6\times10^{10}$ and its rms size $\sigma_{\bar{p}}=0.7$ mm, the tune shift due to electron beam $\xi_e=-0.01$, the distance to the coupling resonance $\Delta\nu=|\nu_x-\nu_y|=0.01$, and the synchrotron tune $\nu_s=0.001$, the instability takes place if the longitudinal magnetic field in the setup is below threshold of about $B_{thr}=17.5$ kG. Essential features of the instability are (1) the constant skew wake plays a major role in the mode coupling; (2) the threshold solenoid field B_{thr} is proportional to the transverse charge density of the electron beam, to the transverse charge density of the antiproton beam, and inversely proportional to the product $\nu_s^{1/2}|\nu_x-\nu_y|^{\kappa}, \kappa\approx1/2$ in the vicinity of the coupling resonance $\nu_x-\nu_y=integer$; (3) a tune spread comparable or larger than ν_s can lead to substantial suppression of the instability.

Rough estimates have shown that having the electron beam transverse size a_e several times wider than the antiproton rms beam size $\sigma_{\bar{p}}$ results in lower threshold magnetic field $B_{thr}\propto(\sigma_{\bar{p}}/a_e)^2$.

We plan to continue investigations of the instability in order to clear some inadequacies of the present studies. In particular, the following effects have to be taken into consideration: (1) nonlinear forces with general current distributions in the electron and antiproton beams; (2) instability suppression due to betatron and synchrotron tune spreads; and (3) higher order transverse mode coupling.

ACKNOWLEDGMENTS

The authors acknowledge stimulating discussions with Vasily Parkhomchuk, Andrei Sery, Gerry Jackson, and David Finley.

[1] J.P. Marriner, FERMILAB-Conf-96/391 (1996); S.D. Holmes *et al.*, FNAL-TM-1920 (1995).
[2] V. Shiltsev and D. Finley, FERMILAB-TM-2008 (1997).
[3] V. Shiltsev, FERMILAB-TM-2031 (1997).
[4] V. Shiltsev, V. Danilov, D. Finley, and A. Sery, FNAL-Pub-98/260 (1998).
[5] G.I. Budker *et al.*, Part. Accel. **7**, 197 (1976).
[6] ''Contributions to the Mini-Workshop on Beam-Beam Compensation,'' edited by V. Shiltsev, FERMILAB-Conf-98/064 (1998).
[7] V. Shiltsev and A. Zinchenko, Phys. Rev. ST Accel. Beams **1**, 064 001 (1998).
[8] A. Chao, *Physics of Collective Beam Instabilities in High Energy Accelerators* (Wiley, New York, 1993).
[9] V.V. Danilov and E.A. Perevedentsev, Nucl. Instrum. Methods Phys. Res. A **391**, 77 (1997).
[10] R.E. Blahut, *Fast Algorithms for Digital Signal Processing* (Addison-Wesley, New York, 1985).
[11] M. Blaskievicz, Phys. Rev. ST Accel. Beams **1**, 044 201 (1998).
[12] A.S. Artamonov and N.I. Inozemtsev, Nucl. Instrum. Methods Phys. Res. A **235**, 13 (1985); V. Danilov, Ph.D. thesis, Budker INP, Novosibirsk, 1995 (in Russian) (unpublished).
[13] D.V. Pestrikov, Nucl. Instrum. Methods Phys. Res. A **373**, 179 (1996).